Saudi Pharmaceutical Journal 29 (2021) 1166–1172

Contents lists available at ScienceDirect

Saudi Pharmaceutical Journal

journal homepage: www.sciencedirect.com

Original article

Adamantane-derived scaffolds targeting the sigma-2 receptor; an *in vitro* and *in silico* study

Mohammed A. Alamri [a,*], Mubarak A. Alamri [b]

[a] Department of Pharmacology and Toxicology, College of Pharmacy, Prince Sattam Bin Abdulaziz University, Al-Kharj 16273, Saudi Arabia
[b] Department of Pharmaceutical Chemistry, College of Pharmacy, Prince Sattam Bin Abdulaziz University, Al-Kharj 16273, Saudi Arabia

ARTICLE INFO

Article history:
Received 12 April 2021
Accepted 23 August 2021
Available online 29 August 2021

Keyword:
Sigma-2 Receptor

ABSTRACT

Novel adamantane-based compounds were synthesized and assessed as potential sigma-2 receptor ligands. Molecular docking and 50 ns molecular dynamic simulation were carried out to determine the binding modes, mechanism of interaction, and stability of these compounds within the active site of the sigma-2 receptor. In addition, the ADME-T properties have been explored. The cytotoxicity in cancer cell lines that express sigma-2 receptors was also examined. In addition, the in silico and cytotoxicity data for the new compounds were compared to a reference sigma-2 receptor ligand with high receptor-binding affinity and selectivity. The data suggests that the new compounds interact with the sigma-2 receptor in a comparable manner to the reference compound, and that adamantane can be used as a scaffold to synthesize sigma-2 receptor ligands with useful functional groups that can be used to conjugate moieties for tumor-imaging or cytotoxic cargo delivery.

1. Introduction

The sigma-2 (σ2) receptor is currently being investigated as a potential target in cancer and Alzheimer's disease, with ongoing clinical trials examining the activity of a σ2 receptor allosteric antagonist against the latter. Research revolving around σ2 receptors showed that ligands had promising anticancer and tumor-imaging abilities, both in vitro and in vivo (Vilner et al., 1995; Kashiwagi et al., 2007; Makvandi et al., 2015). σ2 receptor ligands demonstrated interesting activities, such as the ability to cause apoptotic cell death, undergo endocytosis in cancer cells, and being highly retained within tumor cells compared to normal tissues (Ostenfeld et al., 2005; (Zeng et al., 2007); Shogi et al., 2013). Yet the efforts to understand the nature, crystal structure, and mechanistic pathways for this receptor received less attention, until 2011, when it was suggested that the σ2 receptor is synonymous with PGRMC1 (progesterone receptor membrane component-1) (Xu et al., 2011). However, this identification came under scrutiny and was highly debated by the fact that the latter could not bind the reference σ2 receptor ligand DTG (ditolylguanidine) (Hiranita, 2016; Pati et al., 2017). In addition, PGRMC1 knockout cells did not show a change in susceptibility to σ2 receptor ligands (Zeng et al., 2019). Later on, the σ2 receptor was identified as TMEM97 (transmembrane protein 97), since TMEM97 knockout reduces specific σ2 receptor binding of ^{3}H-DTG (Alon et al., 2017).

Although ambiguity still surrounds the pharmacodynamics of σ2 receptors, the crystal structure of bovine σ2 receptors was successfully determined as an endoplasmic transmembrane homodimer (Alon et al., 2021). And fortunately, the orientation of σ2 receptor ligands within the binding pocket were highly similar in both molecular docking and isolated receptor crystals, lending further credence to computational methods.

Functional assessment of σ2 receptor ligands was previously attempted in literature, contingent upon the ability to induce caspase-3 activation and apoptosis, and it was found that not all ligands with high σ2 receptor affinity cause apoptotic cell death, thus giving a basic functional characterization (agonist/partial agonist/antagonist) to σ2 receptor ligands (Zeng et al., 2014). However, pharmacodynamic uncertainty did not prevent investigators from targeting this receptor with all manner of ligands ranging from radioactive, fluorescent, and covalently-bond anticancer conjugates with promising results (Lee et al., 2016; Makvandi et al., 2016; Alamri et al., 2020a).

* Corresponding author.
E-mail address: ma.alamri@psau.edu.sa (M.A. Alamri).
Peer review under responsibility of King Saud University.

Production and hosting by Elsevier

https://doi.org/10.1016/j.jsps.2021.08.016
1319-0164/

In this study we designed and synthesized adamantane-based compounds that can undergo further chemical modification (N-alkylation, or amide formation) as a backbone for potential future synthesis of dichotomous ligands. We also examined the molecular docking, molecular dynamic (MD) simulation, ADME-T properties, and anticancer activity of these compounds in comparison to a previously discovered σ2 receptor ligand with high receptor-binding selectivity and affinity (σ2 receptor *ki* = 16 nM, σ1 receptor *ki* > 10,000 nM; Alamri et al., 2020a).

2. Materials and methods

2.1. General procedure for organic synthesis and analysis

Reagents used in synthesis and analysis were used with no further processing. All reactions were conducted under nitrogen gas and with anhydrous solvents. All chemical reagents were acquired from Sigma Aldrich (St. Louis, MO, USA) except for 2-adamantanone which was acquired from Beijing Mesochem Technology Co., Ltd (Beijing, China). Flash column chromatography was done using silica gel (230–400 mesh, 60 Å). TLC plates (thin layer chromatography, 1500 μm) were acquired from ANALTECH (Newark, DE, USA). Proton NMR spectra were obtained using CD_3OD (methanol d_4) on a Bruker Ultrashield Plus 500 MHz spectrometer at 24 °C. Chemical shifts (δ) are relative to TMS as ppm. Multiplicity of chemical shifts are s for singlet, d for doublet, t for triplet, and m for multiplet. Coupling constants (*J*) are reported in hertz. Carbon NMR spectra were obtained using a Bruker 700 MHz spectrometer and DMSO d_6 as a solvent. High resolution mass spectrometry (HRMS) was obtained by direct injection on UPLC RS Ultimate 3000 Q Exactive hybrid quadrupole-Orbitrap mass spectrometer (Thermo Scientific) which combines high performance quadrupole precursor selection with high resolution, accurate-mass (HR/AM) Orbitrap™ detection. HMRS parameters: 1 min runtime using nitrogen (auxiliary gas). The flow rate was 5 μL/min. Scan range was from 160 to 1250 *m*/*z*. Resolving Power was set to 70,000 @ *m*/*z* 200. Positive mode was used for detection. Calibration was carried out using Thermo Scientific Pierce™ LTQ Velos ESI Positive Ion Calibration Solution. Capillary temperature was 150 °C and ionization voltage was 3500 V. All ^{1}H NMR and HRMS spectra for the target compounds are in the supplementary data. HPLC analysis was performed using a 250 × 4.6 mm C18 column, a UV detector (270 nm), and a mobile phase consisting of 90:10 methanol and water (0.1% formic acid). All HPLC spectra are listed in the supplementary information.

2.2. Preparation of 2-(4-Fluoro-phenyl)-adamantan-2-ylamine (1)

The reaction began by forming a Grignard's reagent using 57 mmole (6.262 mL) of 4-fluorobromobenzene with 171 mmole (4.156 g) of magnesium in 100 mL THF (tetrahydrofuran) at room temperature. After the reaction cooled down, 62.7 mmole (9.419 g) of 2-adamantanone was added slowly and was left mixing for 2 h. Following this, residual magnesium was decanted and 50 mL acidic water (HCl, pH = 2) and 100 mL ethyl acetate were added. Next, the organic phase was collected, dried over anhydrous Na_2SO_4, and condensed using vacuum to yield the alcohol intermediate as a colorless oil. Following this, the azide intermediate was formed by slowly adding the alcohol intermediate to 114 mmole (7.411 g) of NaN_3 and 171 mmole (13.086 mL) of TFAA (trifluoroacetic acid) in 150 mL chloroform at 25 °C. The reaction was left overnight. Following this, adequate $NaHCO_3$ was added to neutralize the residual TFAA, then the organic phase was dried using Na_2SO_4, then condensed to give a crude yellow oil. Purification was done via flash column chromatography using silica gel as a stationary phase and hexane as an eluant. The product was collected as a colorless oil which crystallized overnight (49.6 mmole, 13.458 g, 87%). Next, compound (**1**) was obtained by reducing 37 mmole (10.039 g) of the azide intermediate using 72 mmole (2.732 g) $LiAlH_4$ powder (lithium aluminum hydride) in THF. After 2 h, excess reducing agent was quenched using a mixture of THF and water (1:1 v/v), then the organic phase was collected, dried over Na_2SO_4, and condensed to give a yellow oil (27.2 mmole, 6.68 g). Following this, purification was carried out using preparative TLC and ethyl acetate as an eluant to yield a colorless oil which was converted to the HCl salt (20.9 mmole, 5.89 g, 56.49%).

HRMS M + H calculated: 246.1658, found: 246.1648

^{1}H NMR (500 MHz, CD_3OD) δ 7.7–7.6 (m, 2H), 7.35–7.2 (m, 2H), 4.64 (s, 6H), 2.82 (s, 2H), 2.25 (d, *J* = 13.5 Hz, 2H), 2.06 (d, *J* = 12.5 Hz, 3H), 1.85 (d, *J* = 13.5 Hz, 7H).

^{13}C NMR (700 MHz, DMSO d_6) δ 26.13, 26.80, 31.17, 32.18, 33.57, 37.66, 61.02, 115.78, 129.84, 135.35, 161.47, 162.86.

HPLC AUC: 99.08%

2.3. Preparation of 2-(4-Fluoro-phenyl)-adamantan-2-ylamine-5-[2-(4-Fluoro-phenyl)-adamantan-2-ylamino]-pentanoic acid ethyl ester (2)

Synthesis was carried out by reacting 1.4 mmole (343 mg) of the base form of amine (**1**) with 4.2 mmole (665 μL) ethyl 2-bromovalerate and 8.4 mmole (1.17 mL) triethylamine in 50 mL acetonitrile at 80 ^{0}C for 24 h. Following this, 50 mL basic water (KOH, pH = 11) was added, then the organic phase was collected, dried over Na_2SO_4, and condensed under vacuum. Purification was carried out using preparative TLC plates, and a mixture of ethyl acetate and hexane (1:1 v/v) as a mobile phase to yield a colorless oil which was converted to the HCl salt (0.414 mmole, 169 mg, 29.6%).

HRMS M + H calculated: 374.2495, found: 374.2482

^{1}H NMR (500 MHz, CD_3OD) δ 7.73–7.71 (m, 2H), 7.32–7.29 (m, 2H), 4.11–4.07 (m, 2H), 2.92 (s, 2H), 2.72–2.68 (m, 2H), 2.33 (d, *J* = 13.5 Hz, 2H), 2.22–2.19 (m, 2H), 2.07 (d, *J* = 14.5 Hz, 3H), 1.88–1.77 (m, 7H), 1.51–1.42 (m, 4H), 1.3–1.2 (m, 3H).

^{13}C NMR (700 MHz, DMSO d_6) δ 14.55, 21.94, 25.53, 25.84, 36.85, 31.05, 33.07, 33.83, 37.65, 41.18, 60.22, 67.49, 116.01, 131.11, 132.21, 161.72, 172.92.

HPLC AUC: 99.66%

2.4. Preparation of N-[2-(4-Fluoro-phenyl)-adamantan-2-yl]-N',N'-dimethyl-propane-1,3-diamine (3)

The reaction was carried out by reacting 0.816 mmole (200 mg) of the base form of amine (**1**) with an equimolar amount (129 mg) of 3-Dimethylamino-1-propyl chloride hydrochloride and 2.45 mmole (341 μL) triethylamine in 50 mL acetonitrile at 130 ^{0}C for 72 h. Following this, the crude mixture was condensed then purified using preparative TLC and a mobile phase composed of methanol and ethyl acetate (1:10 v/v) yielding a clear oil which was converted to the HCl salt (0.033 mmole, 13 mg, 4%).

HRMS M + H calculated: 331.2550, found: 331.2540

^{1}H NMR (500 MHz, CD_3OD) δ 7.78–7.73 (m, 2H), 7.33–7.29 (m, 2H), 3.33–2.94 (m, 4H), 2.83 (s, 8H), 2.45 (d, *J* = 14 Hz, 2H), 2.19–2.08 (m, 5H), 2–1.76 (m, 8H), 1.35–1.25 (m, 2H).

^{13}C NMR (700 MHz, DMSO d_6) δ 8.92, 21.36, 25.87, 26.89, 31.08, 33.86, 37.68, 39.01, 42.35, 45.86, 54.00, 67.76, 116.03, 131.27, 132.08, 161.68, 163.10.

HPLC AUC: 98.6%

2.5. Homology modeling and validation

The 3D structure of human σ2 receptor was built by homology modeling using our previously reported method (Alamri et al.,

2020b). Briefly, the protein sequence of human σ2 receptor amino acids 1–176 (ID: Q5BJF2) in FASTA format was retrieved from UniProtKB database. The 3D structure of σ2 receptor was determined by homology modeling using the I-TASSER (Iterative threading assembly refinement) webserver (https://zhanglab.dcmb.med.umich.edu/I-TASSER/). This hierarchical approach is an integrated online platform for automated protein structure and function prediction starting from the primary amino acid sequence and based on the sequence to structure to function approach (Zhang, 2008). The structure of the mitochondrial translocator protein (PDB ID: 2MGY) was identified to be a closely related protein, so it was used as a template for the structure (Jaremko et al., 2014). The predicted structure contained was composed of 7 α helices. The model was subjected to energy minimization by YASARA Energy Minimization Server (http://www.yasara.org/minimizationserver.htm) using YASARA force field to remove all bad contacts and reduce the model energy globally (Krieger et al., 2002, 2014). This model was validated by several equations including ERRAT, Verify 3D, ProSA, ProQ, QMEAN, and PROCHECK as we reported previously (Alamri et al., 2020b).

2.6. Molecular docking

The molecular docking of synthesized compounds was conducted using Autodock Vina software (Trott and Olson, 2010). The 2D structure of compounds was sketched using ChemDraw Ultra 7.0 software and converted into 3D using OpenBabel 3.0.0 software (O'Boyle et al., 2011). The hydrogen atoms of protein and ligands were added by Autodock Tools and saved in PDBQT format. The auto grid tool was utilized for arrangement affiliation of grid maps and contained 1.00 Å spacing with box dimensions of 20 X × 20 Y × 20 Z Å and centers of 76.160 X × 71.016 Y × 71.999 Z Å. The docking grid box was centered to cover residues within the active site (ASP29 and ASP56) in the protein structure. The interactions of hydrophobicity and hydrogen bonds between the docked compounds and protein were investigated utilizing the Discovery Studio 2019 software, and have been furthermore visualized and analyzed in PyMOL and UCSF Chimera 1.14 in 3D structure.

2.7. Molecular dynamic (MD) simulation

The GROMACS 2018.1 package systems was utilized to simulate the top docked pose of each compound in complex with σ2 receptor using OPLS-AA all-atom force fields using TIP3P water model as described previously (Van Der Spoel et al., 2005). In short, SwissParam web-server was used to generate the ligands topology parameters (Zoete et al., 2011). Each complex was solvated and neutralized by adding 0.15 M of counter Na^+ Cl^- ions in a cubic box with at least 1 nm spacing from the ligand-protein complex. Each complex was then subjected to energy minimization using "steepest descent algorithm". Lenience was 1000 kJ/mol/nm of maximum step size of 0.01 nm. Constraints in bond lengths were applied by "LINear Constraint Solver algorithm" (LINCS) and the electrostatic calculations were conducted using the particle mesh Ewald (PME) method. The complex was then equilibrated for 100 ps using "canonical ensembles NVT" followed by NPT (isothermal–isobaric ensemble). Finally, a 50 ns production run was performed for each system. The preliminary analyses such as root-mean square fluctuations (RMSF), root-mean square deviation RMSD, number of hydrogen-bond (HB), and radius of gyration (Rg) were performed using toolkits of GROMACS 2018.1 package.

2.8. ADME-T calculation

Absorption, distribution, metabolism, excretion, and toxicity (ADME-T) properties were predicted by admetSAR (http://lmmd.ecust.edu.cn:8000/) based on their chemical structures (Cheng et al., 2012). Various absorption parameters, metabolism interactions, and toxicity parameters were assessed.

2.9. NCI-60 human tumor cell lines Screen

Assessment of anticancer activity was conducted by the NCI (National Cancer Institute, USA) according to the published protocol (NCI-60 Human Tumor Cell Lines Screen). Briefly, testing is done using a dose of 10 μM and 48 h incubation time, afterwhich the viability of cells is compared to control to assess growth inhibition using Sulforhodamine-B assay (for more details: https://dtp.cancer.gov/discovery_development/nci-60/methodology.htm).

3. Results and discussion

3.1. Synthesis

The synthesis of target compounds was successfully carried out by forming a Grignard reagent which reacted readily with 2-adamantanone to form the corresponding alcohol, followed by forming the azide intermediate which was then reduced to give the primary amine (compound **1**), this was then alkylated with the appropriate alkylhalides to form compounds **2** and **3** according to the shown scheme (Fig. 1).

The design of the σ2 receptor ligands was based on ligand-based modeling. Hence, previous ligand-based pharmacophore model based on several σ2 receptor binders with high binding affinity (k_i < 1 nM) were shown to be composed of one aromatic ring, one hydrophobic (HY) region, one hydrogen-bond-acceptor group, and one positive ionizable feature (Alamri et al., 2020b).

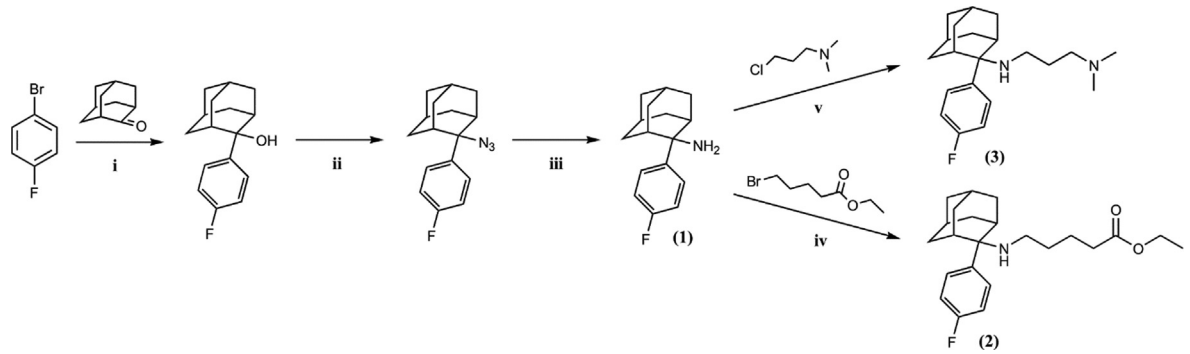

Fig. 1. Synthesis scheme for target compounds. Conditions: **i)** Mg, THF, 25 °C. **ii)** NaN_3, TFAA, CH_3Cl, 25 °C. **iii)** $LiAlH_4$, THF, 25 °C. **iv)** TEA, ACN, 80 °C. **v)** TEA, ACN, 130 °C.

Adamantane was chosen as a scaffold due to its steric hindrance, which may enable better understanding of the binding orientation within the pharmacophore due to increased molecule rigidity, minimizing possible orientations within the binding site. In addition, the bulky nature of adamantane may potentially minimize off-target interactions. These design choices may be advantageous since many of the σ2 receptor ligands in literature have a more flexible nature (Zeng and Mach, 2017). In addition, adamantane derivatives were used previously to target the σ2 receptor, achieving low nanomolar affinity (Riganas et al., 2012). Furthermore, the design of the target compounds enables further chemical modification through N-alkylation or amide formation which may give rise to conjugated ligands for imaging or cytotoxic cargo delivery, similar to a bicycloheptylamine-doxorubicin conjugate previously reported with potent anti-cancer activity in σ2 receptor-expressing cell lines (Alamri et al., 2020a).

3.2. Molecular docking

Assessment of molecular docking was performed to investigate free-binding energy scores as well as the binding conformation of compounds within the active site of σ2 receptor which may give suggestions about their mechanisms of action. Due to the absence of the crystal structure of the σ2 receptor, the molecular docking was carried out against our previously reported homology model of human σ2 receptor (Fig. 2**B**). The docking binding energy scores of synthesized compounds were found to be comparable to the reference compound (Table 1).

The molecular docking results displayed that all compounds adapted a similar binding mode and orientation within the active site of the σ2 receptor (Fig. 2**C**). It was observed that the bicylo [2.2.1]heptane and adamantane ring systems of the reference compound and the synthesized compounds, respectively, bind to the same hydrophobic pocket formed by L26, L38, A64 and W65. Furthermore, the fluorobenzene moiety within all molecules including the reference occupied the adjacent small hydrophobic site formed by V41 and F27 (Fig. 2**C**). These hydrophobic interaction networks were involved in stabilizing the compounds in the active site. The piperidine ring of the reference was found to form a hydrophobic interaction with P23. The primary amine of compound 1 was shown to have a hydrogen bond with L26. Compound 2 and 3 were involved in two fluorine-hydrogen bonds with L38 and W39.

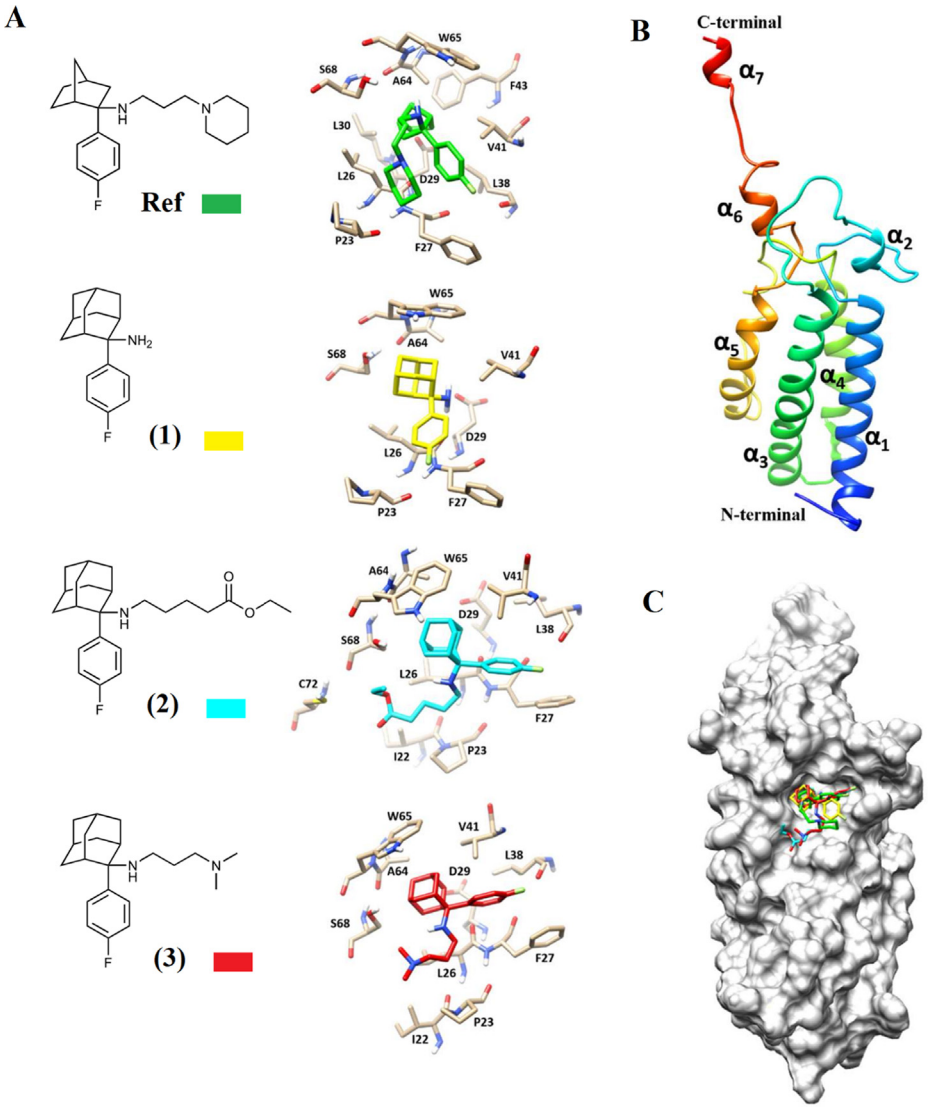

Fig. 2. (**A**) Chemical structures and 3D molecular interaction of reference compound (green), compound 1 (yellow), compound 2 (cyan), and compound 3 (red) with the σ2 receptor. (**B**) The generated homology model of the σ2 receptor. (**C**) Surface representation of the σ2 receptor showing the binding mode.

Table 1
Summary of docking energy scores and types of molecular interaction of the reference and test compounds.

Ligand	Binding energy score (Kcal/mol)	Interaction (H-bond/Hydrophobic)	Close contact residues
Reference	−6.1	Pro23, Leu26, Val41, Ala64	Phe27, Asp29, Trp65, Ser68
1	−7.2	Leu26, Val41, Ala64, Trp65	Pro23, Phe27, Asp29 Ser68
2	−6.8	Leu26, Leu38, Tyr39, Val41, Ala64, Trp65	Ile22, Pro23, Phe27, Asp29, Ser68, Phe69 Cys72
3	−6.8	Leu26, Leu38, Tyr39, Val41, Ala64, Trp65	Ile22, Pro23, Phe27, Asp29, Ser68, Cys72

Importantly, all compounds including the reference were in a close vicinity of the critical residue; Asp29 (Fig. 2**A**). The detailed 2D molecular interaction of ligands with the σ2 receptor are depicted in **Figure. S13**. The obtained data implied that the replacement of bicylo[2.2.1]heptane with adamantane ring system had limited influence on the free-binding energy, as well as the mechanism of interaction of these compounds.

3.3. Molecular dynamic simulation

MD simulation approaches have been proven useful to investigate the binding stability of molecules to biomolecules and predicting the structural basis underlying their molecular mechanisms (Hollingsworth and Dror, 2018). To understand the dynamic stability of synthesized compounds in the active site of the receptor, MD simulation was conducted for 50 ns. The conformation and dynamic changes observed during the 50 ns simulation for the apo-protein (no ligand bound) and in complex with synthesized compounds are discussed herein. To get insight into the dynamic behavior and stability of the apo-protein and ligand-complexes, the backbone "root-mean square deviation" (RMSD) was computed. RMSD is a commonly used parameter to measure the global fluctuations of biomolecules or complexes. Fig. 3**A** showed the backbone RMSD of the σ2 receptor in apo form as well as in complex with compounds. The RMSD of all systems sharply increased during the initial equilibration phase, due to the change in simulation condition, but rapidly converged after ~ 5 ns. The average RMSD values of simulated systems are portrayed in (Table 2). Compound **1** complex displayed the lowest RMSD (0.70 ± 0.08 nm), followed by compounds **2**, **3** and then the reference compound complexes, respectively. Interestingly, the apo-protein displayed higher RMSD of 1.02 ± 0.12 compared to other simulated systems. The data indicate that these compounds provide more dynamic stability to the system upon their binding to the receptor.

The root means square fluctuation (RMSF) is another frequently used parameter to depict the dynamic flexibility of a systm by measuring the mobility of Cα-atoms in each residue in the system around its mean position. With respect to the apo-protein, compound **2** complex had lower RMSF of 0.22 ± 0.12 (Fig. 3**B**). In contrast, compound **3** complex had the highest RMSF of 0.33 ± 0.19 indicating greater fluctuations. The average RMSF values of other systems are listed in (Table 2). Analysis of RMSF showed that the main differences among compound complexes were observed at R44 of α2 helix near the active binding site. The other most fluctuated residues were in the loop region away from the active sites such as K125- E135. Notably, the fluctuation among systems around the key D29 and D56 residues were low comparing to apo-protein. The radius of gyration (Rg) is a parameter to assess the changes in the compactness of a biomolecule. No significant changes were detected for all simulated systems implying sustained stability and compactness of all systems (Fig. 3**B**). Among the compound complexes, compound **3** complex displayed relatively higher Rg of ~2 nm (Fig. 3**C**). Next, the stability of hydrogen bonds (HB) under simulation conditions were computed. HB is an essential factor for a stable ligand–protein complex. Fig. 3**D** showed that compound **1** was found to form up to 2 stable HB with the receptor. Other complexes were able to form 1 HB (Table 2). Overall, our test compounds showed good MD simulation results implying that they may have affinity to σ2 receptors comparable to the reference compound, which was already reported to have high receptor-binding affinity.

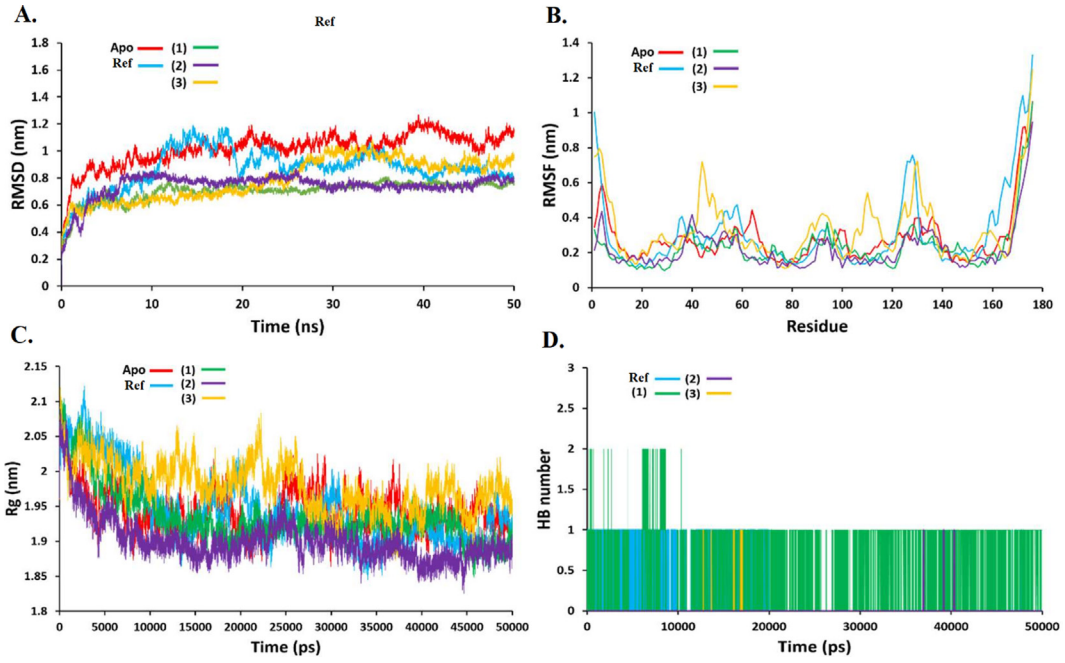

Fig. 3. Comparison of (**A**) Backbone RMSD, (**B**) RMSF values, (**C**) Rg trajectory, and (**D**) Hydrogen bond (HB) interactions over a period of 50 ns of MD simulation of ligand–protein (Apo-protein, reference, and test compounds) complexes.

Table 2
Dynamics stability calculation for σ2 receptor in apo form (no ligand bound) and in complex with compounds during 50 ns MD simulation (Average values presented in nm ± standard deviation).

System	RMSD (nm)	RMSF (nm)	Rg (nm)	HB
Apo	1.02 ± 0.12	0.28 ± 0.15	1.94 ± 0.03	–
Reference	0.87 ± 0.15	0.31 ± 0.22	1.95 ± 0.05	1
1	0.70 ± 0.08	0.23 ± 0.14	1.93 ± 0.04	2
2	0.74 ± 0.09	0.22 ± 0.12	1.90 ± 0.03	1
3	0.79 ± 0.15	0.33 ± 0.19	1.98 ± 0.04	1

3.4. ADME-T properties

ADME-T profiling is an important indicator in determining the pharmacokinetic properties of potential drug molecules. The experimental evaluation of ADME-T is costly and time consuming. Therefore, the prediction of ADME-T properties via computational methods has become the method of choice in early drug discovery (Shen et al., 2010). Hence, the ADME-T properties of three synthesized compounds were calculated using the admetSAR tool (Table 3) (Cheng et al., 2012). The data suggests blood–brain barrier permeability. Although all compounds were also predicted to undergo intestinal absorption, compound **2** showed negative permeability in Caco-2 cells. "Topological Polar Surface Area" (TPSA) and Log P (lipophilicity parameters) of compounds were also calculated. The synthesized compounds showed favorable lipophilicity (log P < 5 and TPSA < 140 Å), indicating adequate penetration of the cell membrane and oral bioavailability (Shukla et al., 2014). All compounds showed distinct metabolic interactions. Only compound **2** showed high cytochrome P450 (CYP450) inhibitory promiscuity, in contrast to compounds **1** and **3**. Compounds **1** and **2** displayed potential inhibition of CYP450 1A2. Although compound **1** was not predicted to be a substrate for P-glycoprotein, compounds **2** and **3** showed a possible interaction with P-glycoprotein. All the synthesized compounds are predicted to lack mutagenic and carcinogenic effects according to the AMES mutagenesis and carcinogens tests. Acute oral toxicity was also assessed displaying compounds **1** and **3** as class III toxins, while compound **2** was classified as class II. In general, these compounds are expected to have favorable pharmacokinetic profiles.

3.5. Anticancer activity

The anticancer activity was assessed in the NCI-60 screening program, the complete data is in the supplementary section. The compiled data on cell lines reported to express σ2 receptors is shown below (Table 4). These cell lines are HT29, A549/ATCC, MAD-MB-468 (Abbas et al., 2020), MAD-MB-435 (Zeng et al., 2007), OVCAR-3 (Peluso et al., 2008), DU-145 (Christy et al., 1999), and MCF7 (Vilner et al., 1995). Our compounds showed varying degrees of growth inihibiton.

Although the cytotoxicity in cell lines expressing σ2 receptors is unremarkable, it is not surprising because many molecules with high receptor-binding affinity showed modest anticancer activity,

Table 3
Predicted ADME-T properties of synthesized compounds.

Properties	Compounds		
	1	2	3
Absorption			
BBB	+ (0.9933)	+ (0.9870)	+ (0.9948)
Human Intestinal absorption	+ (0.9837)	+ (0.9918)	+ (0.9882)
Caco-2 permeability	+ (0.7058)	−(0.5238)	+ (0.7200)
Human oral bioavailability	+ (0.8143)	+ (0.7143)	+ (0.7714)
Log P	3.44	4.80	4.02
TPSA ($Å^2$)	26.02	38.33	15.27
Metabolism			
P-glycoprotein substrate	−(0.7468)	+ (0.5253)	+ (0.7861)
P-glycoprotein inhibitor	−(0.9296)	−(0.4673)	−(0.6532)
CYP450 2C9 substrate	−(1.0000)	−(0.6458)	−(1.0000)
CYP450 2D6 substrate	+ (0.5375)	−(0.7296)	+ (0.6680)
CYP450 3A4 substrate	−(0.6287)	−(0.6525)	−(0.6787)
CYP450 1A2 inhibitor	+ (0.5468)	+ (0.7063)	−(0.6019)
CYP450 2C9 inhibitor	−(0.7227)	−(0.6957)	−(0.9032)
CYP450 2D6 inhibitor	−(0.8239)	−(0.5080)	−(0.5909)
CYP450 2C19 inhibitor	−(0.5000)	−(0.5955)	−(0.9032)
CYP450 3A4 inhibitor	−(0.8931)	−(0.8267)	−(0.6528)
CYP inhibitory promiscuity	−(0.5601)	+ (0.7059)	−(0.8140)
Toxicity			
AMES mutagenesis	−(0.6100)	−(0.7500)	−(0.6400)
Carcinogens	−(0.7714)	−(0.6857)	−(0.9286)
Acute oral toxicity	Class III (0.6929)	Class II (0.4375)	Class III (0.5482)

BBB: blood brain barrier; CYP450: cytochrome P450. "Acute oral toxicity" is classified according to the US Environmental Protection Agency criteria. Class I: LD50 value is ≤ 50 mg/kg; Class II: LD50 value is > 50 to 500 mg/kg; Class III: LD50 value is > 500 to 5000 mg/kg. The probability of each property was highlighted between brackets.

Table 4
Growth % in cell lines that express σ2 receptors relative to control (10 μM, 48 h).

	Reference	Compound 1	Compound 2	Compound 3
HT29	48.09	96.51	84.86	67.64
MCF7	87	88.36	89.01	81.93
T-47D	84.17	100.49	97.46	88.46
MDA-MB-468	77.5	98.68	98.79	83.35
MDA-MB-435	83.24	104.12	101.26	93.22
A549/ATCC	103.09	98.06	103.15	96.98
OVCAR-3	92.7	124.85	121.68	103.45
DU-145	104.56	122.02	115.1	103.95

since not all ligands necessarily possess cytotoxic activity, as is the case with previously reported fluorescent and radio-labeled σ2 receptor ligands (Kashiwagi et al., 2007; Zeng et al., 2007; Makvandi et al., 2016; Pati et al., 2017).

4. Conclusion

The molecular docking and MD simulation data suggest that our adamantane-based compounds bind within the active site of the σ2 receptor in a comparable manner to the reference compound. Furthermore, these compounds are predicted to have appropriate ADME-T profiles. The modest anticancer activity exhibited by the reference and test compounds may suggest antagonistic activity or weak agonistic activity and merits further investigationof functional characteristics. Overall, our data suggest that adamantane-based scaffolds can be made to target the σ2 receptor, and that they can be considered bioisosteres of the reference compound. Adamantane-based ligands may provide a useful backbone to design σ2 receptor ligands as research tools or potential therapeutics and imaging-agents.

Declaration of Competing Interest

The authors declare that they have no known competing financial interests or personal relationships that could have appeared to influence the work reported in this paper.

Acknowledgement

We thank the Deanship of Scientific Research (DSR), at Prince Sattam bin Abdulaziz University, Al-Kharj, Saudi Arabia for providing the funding for this research (grant 9566/03/2019). The authors are also grateful to Mr. Mohamad Ayman Salkini for HRMS and HPLC analysis, and Mr. Anzarul Haque Anwarul Haque for NMR analysis. NCI's Developmental Therapeutics Program is gratefully acknowledged for conducting the NCI-60 Human Tumor Cell Lines Screen.

Appendix A. Supplementary material

Supplementary data to this article can be found online at https://doi.org/10.1016/j.jsps.2021.08.016.

References

Abbas, H., Brode, P., Willars, G.B., Ferry, D.R., Safrany, S.T., 2020. Hazards of Using Masking Protocols When Performing Ligand Binding Assays: Lessons from the Sigma-1 and Sigma-2 Receptors. Front. Pharmacol. 11, 309.

aAlamri, M., Ates-Alagoz, Z., Adejare, A., 2020. Bicycloheptylamine-Doxorubicin Conjugate: Synthesis and Anticancer Activities in σ2 Receptor-Expressing Cell Lines. Med. Chem. 16, 192-201.

bAlamri, M.A., Afzal, O., Alamri, M.A., 2020. Computational screening of natural and natural-like compounds to identify novel ligands for sigma-2 receptor. SAR QSAR Environ. Res. 11, 837-856.

Alon, A., Schmidt, H.R., Wood, M.D., Sahn, J.J., Martin, S.F., Kruse, A.C., 2017. Identification of the gene that codes for the σ2 receptor. Proc. Natl. Acad. Sci. USA 114, 7160–7165.

Alon, A., Lyu, J., Braz, J.M, Tummino, T.A., Craik, V., O'Meara, M.J., Webb, C.M., Radchenko, D.S., Moroz, Y.S., Huang, X., Liu, Y., Roth, B.L., Irwin, J.J., Basbaum, A. I., Shoichet, B.K., Kruse, A.C., 2021. Crystal structures of the σ2 receptor template large-library docking for selective chemotypes active in vivo. bioRxiv. https://doi.org/10.1101/2021.04.29.441652.

Cheng, F., Li, W., Zhou, Y., Shen, J., Wu, Z., Liu, G., Lee, P.W., Tang, Y., 2012. admetSAR: a comprehensive source and free tool for assessment of chemical ADMET properties. J. Chem. Inf. Model. 52, 3099–3105.

Christy, S., Vilner, B.J., Geyer, B.C., Moody, T., Bowen, W.D., 1999. Targeting sigma receptor-binding benzamides as in vivo diagnostic and therapeutic agents for human prostate tumors. Cancer Res. 59, 4578–4583.

Hiranita, T., 2016. Identification of the sigma-2 receptor: Distinct from the progesterone receptor membrane component 1 (PGRMC1). J. Alcohol. Drug. Depend. 4, e130.

Hollingsworth, S.A., Dror, R.O., 2018. Molecular Dynamics Simulation for All. Neuron 6, 1129–1143.

Jaremko, L., Jaremko, M., Giller, K., Becker, S., Zweckstetter, M., 2014. Structure of the mitochondrial translocator protein in complex with a diagnostic ligand. Science. 343, 1363–1366.

Kashiwagi, H., McDunn, J.E., Simon Jr., P.O., Goedegebuure, P.S., Xu, J., Jones, L., Chang, K., Johnston, F., Trinkaus, K., Hotchkiss, R.S., Mach, R.H., Hawkins, W.G., 2007. Selective sigma-2 ligands preferentially bind to pancreatic adenocarcinomas: applications in diagnostic imaging and therapy. Mol. Cancer. 6, 48.

Krieger, E., Koraimann, G., Vriend, G., 2002. Increasing the precision of comparative models with YASARA NOVA—a self-parameterizing force field. Proteins. 47, 393–402.

Krieger, E., Vriend, G., 2014. YASARA View molecular graphics for all devices from smartphones to workstations. Bioinformatics 30, 2981–2982.

Lee, I., Lieberman, B.P., Li, S., Hou, C., Makvandi, M., Mach, R.H., 2016. Comparative evaluation of 4 and 6-carbon spacer conformationally flexible tetrahydroisoquinolinyl benzamide analogues for imaging the sigma-2 receptor status of solid tumors. Nucl. Med. Biol. 43, 721–731.

Makvandi, M., Tilahun, E.D., Lieberman, B.P., Anderson, R., Zeng, C., Xu, K., Hou, C., McDonald, E.S., Pryma, D.A., Mach, R.H., 2015. The sigma-2 receptor as a therapeutic target for drug delivery in triple negative breast cancer. Biochem. Biophys. Res. Commun. 467, 1070–1075.

Makvandi, M., Lieberman, B.P., LeGeyt, B., Hou, C., Mankoff, D.A., Mach, R.H., Pryma, D.A., 2016. The pre-clinical characterization of an alpha-emitting sigma-2 receptor targeted radiotherapeutic. Nucl. Med. Biol. 43, 35–41.

NCI-60 Human Tumor Cell Lines Screen https://dtp.cancer.gov/discovery_development/nci-60/methodology.htm

O'Boyle, N.M., Banck, M., James, C.A., Morley, C., Vandermeersch, T., Hutchison, G.R., 2011. Open Babel: An open chemical toolbox. J. Cheminformatics. 3, 1–14.

Ostenfeld, M.S., Fehrenbacher, N., Høyer-Hansen, M., Thomsen, C., Farkas, T., Jaattela, M., 2005. Effective tumor cell death by σ-2 receptor ligand siramesine involves lysosomal leakage and oxidative stress. Cancer Res. 65, 8975–8983.

Pati, M.L., Groza, D., Riganti, C., Kopecka, J., Niso, M., Berardi, F., Hager, S., Heffeter, P., Hirai, M., Tsugawa, H., Kabe, Y., Suematsu, M., Abate, C., 2017. Sigma-2 receptor and progesterone receptor membrane component 1 (PGRMC1) are two different proteins: Proofs by fluorescent labeling and binding of sigma-2 receptor ligands to PGRMC1. Pharmacol. Res. 117, 67–74.

Peluso, J.J., Liu, X., Saunders, Claffey, K.P., 2008. Phoenix Regulation of ovarian cancer cell viability and sensitivity to cis-platin by progesterone receptor membrane component-1. J. Clin. Endocrinol. Metab. 93, 1592-1599.

Riganas, S., Papanastasiou, I., Foscolos, G.B., Tsotinis, A., Dimas, K., Kourafalos, V.N., Eleutheriades, A., Moutsos, V.I., Khan, H., Margarita, P., Georgakopoulou, S., Zaniou, A., Theodoropoulou, M., Mantelas, A., Pondiki, S., Vamvakides, A., 2012. New adamantane derivatives with sigma affinity and antiproliferative activity. Med. Chem. 8 (4), 569–586.

Shen, J., Cheng, F., Xu, Y., Li, W., Tang, Y., 2010. Estimation of ADME properties with substructure pattern recognition. J. Chem. Inf. Model. 50, 1034–1041.

Shogi, K.I., Xu, J., Su, Y., He, J., Rowland, D., Yan, Y., Garbow, J.R., Tu, Z., Jones, L.A., Higashikubo, R., Wheeler, K.T., Lubet, R.A., Mach, R.H., Yoy, M., 2013. Quantitative receptor-based imaging of tumor proliferation with the sigma-2 ligand [18F]ISO-1. PLoS One. 8, e74188.

Shukla, A., Sharma, P., Prakash, O., Monika, S., Kalani, K., 2014. PLoS ONE 9, 1–14.

Trott, O., Olson, A.J., 2010. AutoDock Vina: improving the speed and accuracy of docking with a new scoring function, efficient optimization, and multithreading. J. Comput. Chem. 31, 455–461.

Vilner, B.J., John, C.S., Bowen, W.D., 1995. Sigma-1 and sigma-2 receptors are expressed in a wide variety of human and rodent tumor cell lines. Cancer Res. 55, 408–413.

Van Der Spoel, D., Lindahl, E., Hess, B., Groenhof, G., Mark, A.E., Berendsen, H.J., 2005. GROMACS: Fast, flexible, and free. J. Comput. Chem. 26, 1701–1718.

Xu, J., Zeng, C., Chu, W., Pan, F., Rothfuss, J.M., Zhang, F., Tu, Z., Zhou, D., Zeng, D., Vangveravong, S., Johnston, F., Spitzer, D., Chang, K.C., Hotchkiss, R.S., Hawkins, W.G., Wheeler, K.T., Mach, R.H., 2011. Identification of the PGRMC1 protein complex as the putative sigma-2 receptor binding site. Nat. Commun. 2, 380.

Zeng, C., Vangveravong, S., Xu, J., Chang, K.C., Hotchkiss, R.S., Wheeler, K.T., Shen, D., Zhuang, Z., Kung, H.F., Mach, R.H., 2007. Subcellular localization of sigma-2 receptors in breast cancer cells using two-photon and confocal microscopy. Cancer Res. 67, 6708–6716.

Zeng, C., Rothfuss, M.J., Zhang, J., Vangveravong, S., Chu, W., Li, S., Tu, Z., Xu, J., Mach, R.H., 2014. Functional assays to define agonists and antagonists of the sigma-2 receptor. Anal. Biochem. 448, 68–74.

Zeng, C., Mach, R.H., 2017. The Evolution of the Sigma-2 (σ2) Receptor from Obscure Binding Site to Bona Fide Therapeutic Target. Adv. Exp. Med. Biol. 964, 49–61.

Zeng, C., Weng, C.C., Schneider Jr., M.E., Puentes, L., Riad, A., Xu, K., Makvandi, M., Jin, L., Hawkins, W.G., Mach, R.H., 2019. TMEM97 and PGRMC1 do not mediate sigma-2 ligand-induced cell death. Cell Death Discov. 5, 58.

Zhang, Y., 2008. I-TASSER server for protein 3D structure prediction. BMC Bioinfo. 9, 40.

Zoete, V., Cuendet, M.A., Grosdidier, A., Michielin, O., 2011. SwissParam: A fast force field generation tool for small organic molecules. J. Comput. Chem. 32, 2359–2368.